Main Manuscript for

Towards CO Methanation at Mild Conditions on Dual-site Catalysts

Wanghui Zhao^{a,b,1}, Gaomou Xu^{a,b,1}, Zhaochun He^a, Cheng Cai^{a,b}, Frank Abild-Pedersen^c,

Tao Wang^{a,b,*}

^aCenter of Artificial Photosynthesis for Solar Fuels and Department of Chemistry, School of Science, Westlake University, 600 Dunyu Road, Hangzhou 310030, Zhejiang Province, China.

^bInstitute of Natural Sciences, Westlake Institute for Advanced Study, 18 Shilongshan Road, Hangzhou 310024, Zhejiang Province, China.

^cSUNCAT Center for Interface Science and Catalysis, SLAC National Accelerator Laboratory, Menlo Park, CA 94025, USA.

¹These authors contributed equally to this work.

*Tao Wang

Email: twang@westlake.edu.cn

Author Contributions: T.W. supervised this project; W.H.Z., Z.C.H., and C.C. did the DFT computations; G.M.X. performed micro-kinetics modeling and data analysis; T.W. and F.A-P. conceived the idea behind the project; all authors discussed and analyzed the results and contributed to the writing of the manuscript.

Competing Interest Statement: The authors declare no competing interest.

Classification: PHYSICAL SCIENCES, Chemistry

Keywords: Methanation, confined dual-site, Mild-condition, microkinetic modeling, DFT

Abstract

The catalytic CO methanation reaction is an ideal model reaction for the fundamental understanding of catalysis on the gas-solid interface and is crucial for various industrial processes. However, the harsh operating conditions make the reaction unsustainable, and the limitations set by the scaling relations primarily between the energy barrier for CO dissociation and CO dissociative adsorption energy further increase the difficulty in designing high-performance methanation catalysts operating under milder conditions. Herein, we proposed a theoretical strategy to achieve both facile CO dissociation and C/O hydrogenation on a catalyst containing a

confined dual-site, which provides an elegant approach to circumvent the limitations introduced by the scaling relations. Our DFT-based microkinetic modeling reveals that a Co-Cr₂/G dual-site catalyst introduced in this work could provide 4-6 orders of magnitude higher turnover frequency (TOF) for CH₄ production than the cobalt step sites at the same reaction conditions. We believe that the proposed strategy in the current work will provide essential approaches for designing state-of-the-art catalysts for methanation under mild conditions.

Significance Statement

Achieving milder operation conditions is important for the thermal-catalytic methanation process. Unfortunately, the inertness of CO signified through the scaling relation between the CO dissociation energy barrier and CO dissociative adsorption energy makes it very difficult to design high-performance catalysts that can produce methane from CO at low temperatures. In this work, we have shown using DFT how a 4-6 orders of magnitude increase in CH₄ production rate compared with the cobalt step sites can be achieved through facile CO dissociation and C/O hydrogenation on a Co-Cr₂/G dual-site catalyst. This work provides an elegant strategy for fine-tuning bond-breaking and bond-making reactions on confined sites to achieve better catalysts for complex reactions.

Introduction

Since it was discovered by Sabatier and Senderens in 1902, the catalytic CO_x hydrogenation to methane (methanation) has served as an ideal model reaction for the fundamental understanding of catalysis on the gas-solid interface (1). This reaction plays an essential role in various industrial processes such as CH_4 production, CO_x removal in hydrogen purification for fuel cells and ammonia synthesis processes (2). Due to the advancements in the exhaust gas recirculation infrastructure (see Figure 1A) (3, 4), further development of a sustainable CH_4 synthesis from CO_2 or CO derived from CO_2 provides a meaningful addition to the global energy system. With the rapid development of sustainable energy-driven water electrolysis (5, 6) and an economically viable reduction of CO_2 to CO (7–9), the green H_2 -based CO methanation cycle shown in Figure 1A holds the potential to close the carbon cycle and therefore impact the roadmap towards carbon neutrality.

The conversion of CO to methane is mainly limited by challenges associated with the breaking of the strong C-O bond and thus the reaction runs at high temperatures to overcome this barrier. Like the Haber-Bosch process, the methanation reaction is an exothermic reaction (1, 10) and hence the increased total pressure is needed to shift to higher equilibrium conversion at elevated temperatures as seen in Figure 1B (11). Altogether, this will increase the energy consumption of the reaction, introduce higher demands on the pressure resistance of the reactor, the temperature resistance of the catalyst, and also require efficient solutions for heat transfer properties of the reactor (12, 13). Therefore, developing a low-temperature solution for the methanation reaction is one of the key scientific challenges to be resolved and this clearly requires a more energy efficient catalyst.

The search for better catalysts for the methanation reaction has been ongoing since its discovery in 1902 (1). In the work by Vannice et al. (14) an experimental CO to methane activity trend was established across the transition metals Ru, Fe, Ni, Co, Rh, Pd, and Pt, where the metals are arranged in descending order according to activity. Industrially, Co- and primarily Ni-based formulations are the catalyst of choice for the methanation reaction due to their abundance, acceptable activity, and lower cost than Ru, and for that reason also the most thoroughly studied (15, 16). Even though Fe is identified as a high-activity material, it suffers from poor selectivity (17).

One of the challenges with Ni-based catalysts is that they experience fast deactivation via sintering under the high-temperature conditions of the methanation reaction (18, 19). Achieving a suitable Ni-support interaction to avoid sintering and developing a low-temperature methanation strategy is an active area of research (20, 21). Different supports including Al₂O₃ (22), ZrO₂ (23), CeO₂ (24), SiO₂ (25), Y₂O₃ (26), metal-organic frameworks (27) have been systematically evaluated, while CeO₂ and ZrO₂ were identified as good supports for the methanation reaction at 613.15 K and 573.15 K (28). A Ni/ZrO₂-CP (29) catalyst was reported to have 100% CH₄ selectivity at 493.15 K for 100 h in CO methanation and a bimetallic NiCo/SiO₂ (30) catalyst showed stable operation for 100 h at 653.15 K with superior CO conversion and CH₄ selectivity.

Many research groups have reported theoretical simulations providing an essential mechanistic understanding of the methanation reaction, which combined with extensive modeling of rates has guided the catalyst design. For example, Nørskov and coworkers (31) established a computational framework combining DFT and micro-kinetics modeling (MKM) to screen optimal methanation catalysts and the group successfully identified a Fe-Ni alloy as a promising candidate. Studt et al. (32) found that the methanation activity trends of transition metals could be preserved when including the interaction effects in the MKM. A mechanistic study of methanation by Chorkendorff et al. (33) revealed the importance of step sites in dissociating the CO molecule, while the presence of H could change the dissociation path and greatly reduce the energy barrier. Li et al. (34) reported a more favorable H-assisted CO dissociation pathway than CO direct dissociation on Co(0001) surface. Wang et al. (35) demonstrated that Zr-modified Ni(211) has a better methanation performance than pure Ni(211), which is attributed to the higher d-state of step Zr and stronger interactions with HCO, CH₂OH, and CH₃OH. Francis et al. (36) computationally investigated the CO dissociation and methanation on strained Ni(211), Ni₃Fe(211) and NiFe(112) surfaces, and identified strain engineering as an alchemical tool to properly tune catalyst activity. More recently, Andersen et al. (37) used advanced data science and machine learning methods to achieve accurate screening of CO methanation catalysts at a very low computational cost.

Strategies to achieve higher rates of methane production under milder conditions is one of the grand challenges in catalysis but facing severe difficulties since most catalysts still require temperatures above 550 K to effectively activate the strong bond in CO. Clearly, designing a stable catalyst capable of breaking the C-O and simultaneously forming the C-H bond with low energy barriers represents an effective approach. Recently, we proposed a model catalyst with a dual active site capable of activating the inert N \equiv N bond under mild conditions (38), an approach that also appears suitable to address the challenge in CO methanation. As indicated in Figure 1C, the C-O bond will be activated by the dual-site catalyst through the enhanced π back-donation. However, the optimal composition of the dual-site catalyst for CO methanation is still elusive.

In this work, we have set up model structures for dual-sites on twelve different transition metal (Ag, Au, Co, Cu, Ir, Ni, Os, Pd, Pt, Re, Rh, and Ru) catalysts as shown in Figure 1D and have evaluated the intermediates in the CO methanation mechanism. The goal is to identify the optimal metal pairs capable of breaking the C-O bond and simultaneously hydrogenating *C/*O with low energy barriers, which is required for achieving high methanation rates under mild operation conditions. For comparison, we have performed calculations on the reaction network for CO hydrogenation to CH₄ and CH₃OH on the stepped model surfaces of several transition metals. Our results show that a much lower energy barrier for CO dissociation can be achieved on the catalysts with dual sites than on step sites. We eventually identify based on our DFT-based microkinetic modeling a Co/Cr-based dual-site catalyst that shows a 4-6 orders of magnitude higher turnover frequency (TOF) for CH₄ than the step sites on a Co catalyst at the same reaction conditions. We

believe that the site engineering strategy proposed in the current work will provide guidelines for designing state-of-the-art catalysts for CO methanation and other related chemistries.

Results

CO Hydrogenation Reaction Mechanism on Undercoordinated Step Sites. In Figure 2, the mechanisms studied for the CO hydrogenation to methane and methanol are shown. The dissociative CO pathway leads to methane only whereas the associative CO pathway can lead to both methane and methanol. In the dissociative pathway, CO firstly dissociates into surface C (*C) and O (*O) species, followed by the subsequent hydrogenation to CH₄ and H₂O. However, the high energy barrier for C≡O bond breaking makes it difficult and it usually represents the ratedetermining step (RDS) (39). For the associative pathway, CO hydrogenation occurs prior to any dissociation, and it produces intermediate *COH or *CHO depending on the location of the first hydrogenation. Starting from the *COH intermediate, subsequent hydrogenation of the C-side will produce the formaldehyde isomer *CHOH, hydroxymethyl *CH2OH, and finally methanol. The C-O bond breaking could happen for any of the intermediates *COH, *CHOH, and *CH2OH followed by the hydrogenation of CH_x and OH_x to form methane and water. Starting from the *CHO species, one more hydrogenation on the C end will lead to the formation of formaldehyde and the consecutive hydrogenation steps produce methoxy and finally methanol. Methane formation is also possible if the C-O bond breaking occurs within the *CHO, *CH₂O, and *CH₃O intermediates. Clearly, this reaction is very complex and the design of a catalyst with high selectivity to a single product represents a grand challenge.

We have performed systematic DFT calculations of the above reaction networks on stepped model surfaces of 12 transition metals (TMs=Ag, Au, Co, Cu, Ir, Ni, Os, Pd, Pt, Re, Rh, and Ru). The energies are summarized in Table S1 of the supporting information and the cartesian coordinates of all optimized structures are provided in the supporting dataset. For the CO methanation reaction, the dissociative pathway is not competitive on most metals due to the high energy barriers for CO dissociation, ranging from 1.85 eV for the reactive metal Rh to 6.43 eV for the least reactive metal Ag. Despite the facile CO dissociation on Re, the very high energy barriers for the hydrogenation of intermediates *CH_x and *O greatly limits the rate and increases the energy consumption of the reaction. We note that CH₄ formation via the H-assisted associative pathway generally has lower energy barriers but for some of the late transition metals it competes with the production of CH₃OH making the control of selectivity very challenging.

Microkinetic Modeling (MKM) and the Sabatier Principle. Based on the calculated energetics, we established a mean-field microkinetic model to analyze the activity and selectivity of each metallic catalyst at 523 K, p_{CO} = 1 bar, p_{H2} = 2 bar (for details on the MKM we refer to the supporting information). As seen in Figure 3A, metallic Ag, Au, and Cu mainly produce methanol, Pd and Pt show competitive production of CH₄ and CH₃OH, while the more reactive metals mainly produce CH₄. Through a compromise between capital cost and reactivity, catalysts based on Co and Ni have proven to be the best choices for the production of CH₄ from CO among the 12 metals. The selectivity of Co is found to be slightly better than Ni, but of the two Ni is more competitive in terms of price. The Sabatier principle best illustrates how the CO methanation activity of metallic catalysts is restricted by a balance between CO dissociation and further hydrogenation of the intermediate surface *C/*O species (31). In Figure 3B, we show that there is a clearly linear scaling relation between the calculated CO dissociation barriers (E_{C-O}) and CO dissociative adsorption energies (ΔE_{C-O}) (40) on the (211) step sites. When combined with a mean-field MKM, a volcano-shaped relationship between the calculated TOF of methane production (TOF_{CH4}) and ΔE_{C-O} can be plotted. This is seen in Figure 3C, which shows how reactive metals are limited by the hydrogenation of

surface species whereas less reactive metals are limited by the breaking of the strong C-O bond as represented by the Sabatier principle (41). Evidently, Co and Ni with moderate C and O binding strengths are very close to the top of the activity volcano, indicating their good performance for CH₄ production which also agrees well with experimental results (42, 43).

Activation and Hydrogenation of CO on Confined Dual-Site Catalysts. Based on previous work focusing on N₂ activation (38), the dual-site catalysts have the prospect of dramatically decreasing the energy needed to break strong chemical bonds via an enhanced π back-donation. This would provide an elegant strategy to circumvent linear scaling relations, which per definition are tied entirely to one surface. To evaluate reaction barriers for the CO methanation reaction we modeled the dual-site catalysts like the structures shown in the schematics of Figure 1D for the 12 different transition metals. Subsequently, we identified the optimal distance between dual sites through systematic calculations of the barriers for the CO dissociation as well as the following hydrogenation steps towards methane (Figure S1). The TOF_{CH4} was then calculated using the mean-field MKM based on the energetics on the dual sites. As shown in Figure 3B, the dual-site catalysts have much lower CO dissociation energy barriers than the step sites, which significantly enhances the CH₄ production for transition metals where the methanation reaction is limited by the C-O bond breaking step. The dual-site catalysts are seen to obey a different linear scaling relation than the step sites, thus resulting in a new volcano, shown in Figure 3C, where strong binding materials are limited by desorption rates that more resembles the close-packed (111) surface and weaker binding metals which are boosted by the higher rates of CO dissociation. Generally, we find that the dual sites have higher TOF_{CH4} than the step sites, which suggests that the proposed strategy of activating inert chemical bonds by separating the active site components participating in the reaction is valid. Among all the dual-site catalysts, Ir is identified as the catalyst material with the highest TOF_{CH4}, but it is less attractive due to its scarcity. The confined Co and Ni dual-site catalysts are also both very close to the top of the volcano, displaying 2 and 4 orders of magnitude higher TOF_{CH4} than their stepped model surfaces, respectively. In addition to the enhancement in activity, the CH₄ selectivity was significantly improved owing to the favorable dissociative mechanism on such confined dual-site catalysts. Evidently, confined dual-site - e.g. on a Co catalyst structure are theoretically predicted to be promising candidates if one wants to achieve active catalysts for the methanation reaction operating under milder conditions.

Catalyst Design by Tuning the C and O Binding Energies on Confined Dual-site. As shown in Figure 3C, there is still enough space to further optimize the Co-based dual-site catalyst to reach the peak of the volcano. Considering this, we further analyzed the potential energy diagram of the confined Co dual site catalyst for CO methanation shown in Figure S2 and Table S2. It is found that the hydrogenation of CH_x on the Co site with low energy barriers is very smooth, while the OH hydrogenation to H₂O with the highest energy barrier is the rate-limiting step. Therefore, if we could identify an active center (AC) with a slightly weaker O binding that simultaneously retains the capability of breaking the C-O bond with a low energy barrier, then such an integrated Co-AC dualsite system should result in a further increase in CO methanation activity. Clearly, the close-packed surfaces of the early transition metals such as Fe, Mn, Cr, Mo, and W with very strong O binding are unsuitable to represent the active center despite the high rates of dissociating CO and abundance of these metals. Nevertheless, achieving both facile CO dissociation and C/O hydrogenation by tuning the coordination environments of the active center should be possible. We studied the metal-doped graphene as a candidate for the active center of the Co-AC dual-site catalysts. First, the right metal to achieve the aforementioned goals needs to be identified, where Cr, Mn, Fe, Mo, and W with strong metallicity were chosen to represent the single active site on graphene and paired with the Co(111) surface to form the Co-M₁/graphene dual-site catalyst (Co M_1/G) shown in Figure S3. Unfortunately, our calculated energy barriers for CO dissociations on these five Co- M_1/G dual-site catalysts are 2.72 eV (Fe), 2.29 eV (Mn), 1.22 eV (W), 1.87 eV (Cr), and 1.71 eV (Mo), indicating the difficulties in breaking the C-O bond when the site ensemble is too small and therefore unable to accommodate the electronic structure changes associated with the bond breaking. We thus constructed another model catalyst with a larger active site ensemble by anchoring two metal centers on the graphene (Co- M_2/G) as shown in Figure 3D. The calculated CO dissociation energy barriers on these larger active sites are 2.53 eV (Fe), 2.13 eV (Mn), 1.16 eV (W), 1.12 eV (Cr), and 1.41 eV (Mo). In addition, we calculated the binding energies of *O and * H_2 O as well as the energy barriers for the hydrogenation of O/OH on these five metals to ensure the facile production of water (Table S3). Among the five considered Co- M_2/G catalysts, the Co- Cr_2/G was identified as the structure with the lowest barrier for CO dissociation (E_a =1.12 eV) and suitable oxygen chemistry *O (E_a =0.82 eV) and *OH (E_a =0.84 eV) thus representing a very promising candidate for achieving higher methanation activity.

To quantify the enhanced activity of the proposed catalyst, we calculated and compared the TOF_{CH4} on the stepped Co(211) surface, the confined Co dual-site catalyst, and the Co-Cr₂/G system. As shown in Figure 4, the different structures represented by the three catalysts show very distinct activities for the methanation reaction. At the same reaction conditions, the Co-Cr₂/G catalyst show 4-6 orders of magnitude higher TOF_{CH4} than the stepped Co surface. Evidently, the introduction of confinement effects can lead to significant improvements in activity and thus provide essential approaches for designing state-of-the-art catalysts operating under milder reaction conditions.

Conclusion

In summary, we did systematic DFT calculations for the CO hydrogenation mechanism to methane and methanol on model stepped surfaces and confined dual-site for 12 transition metals. Based on the comprehensive dataset, a microkinetic model was established which revealed that for a given metal the confined dual sites generally have more than 2 orders of magnitude higher methane turnover frequency than undercoordinated step sites. This indicates that confinement can stabilize the transition state for bond breaking of otherwise inert reactants effectively and thereby enhance the activity of materials limited by dissociation. The duality of the confined site enables us to integrate two distinct active components to tune the activity even further - the proposed Co-Cr₂/G catalyst is designed to achieve both facile CO dissociation as well as C/O hydrogenation, thus allowing us to circumvent the restrictions set by the linear scaling relations for CO methanation. The theoretically calculated TOF_{CH4} for the Co-Cr₂/G dual-site catalyst is 4-6 orders of magnitude higher than what can be achieved for the Co(211) step sites. Clearly, such improvement in activity allows us to operate the methanation reaction under milder conditions and still achieve a similar TOF. The proposed confined dual-site strategy will help guide the design of new catalysts capable of activating inert chemical bonds at milder conditions, thus leading to more sustainable process solutions in heterogeneous catalysis.

Materials and Methods

Computational details. All DFT calculations were performed using the plane-wave based Vienna ab initio simulation package (VASP) (44) within the Atomic Simulation Environment (ASE) (45). The Bayesian error estimation functional with van der Waals correlation (BEEF-vdW) (46) was used to describe the exchange-correlation functional because of the reasonable ability to describe chemical adsorption on metal surfaces (47). The projected augmented wave (PAW) (48) method was used to describe the interaction between ion cores and valence electrons, combined with the plane wave at an energy cutoff of 400 eV. The stepped surface [the (211) facet for FCC metal] was

simulated with 8-layer (2 × 2) supercells with the topmost four layers relaxed and the bottom four layers constrained. A 4 × 4 × 1 Monkhorst-Pack k-point grids were applied for describing the Brillouin zone. A vacuum of 12 Å is set between two periodic repeated slabs for the normal metal surfaces without confinement. To construct the confined dual-site catalysts with metals, the closepacked surface (the (111) facet for FCC metal, the (110) facet for BCC metal, and the (0001) facet for HCP metal) is used and different values of distance ranging from 12 Å to 4 Å were considered to identify the optimal distance of each metal to form effective bindings with both C and O end of CO molecule, i.e., 4.2 Å for Au, 4.4 Å for Os and Ru, 4.5 Å for Ni, Pt and Re, 4.6 Å for Ag, Cu and Pd, 4.7 Å for Rh, 4.8 Å for Ir, and 4.9 Å for Co. The confined dual-site catalyst shown in Figure S1 was simulated using a 7-layer (2 × 2) supercell with the topmost and bottom two layers relaxed, and the middle three layers constrained. The 4 × 4 × 1 Monkhorst–Pack k-point grids were applied to describe the Brillouin zone. For the Co-M₂/G dual-site catalyst shown in Figure S4, a 4-layer-(4 × 4) supercell of Co (111) was used for the one substrate, and the bottom two layers were fixed during the optimization, while the (4 × 4) supercell of graphene was used as the other substrate of the dual-site catalysts, and the lattice mismatch between these two supercells is less than 2%. For geometry optimization, the force and energy convergence criteria were set to 0.05 eV/Å and 10⁻⁵ eV, respectively. Spin polarization was applied for calculation on Fe, Co, and Ni systems to correctly describe magnetic properties. The transition state (TS) energies for the intermediates and target products were calculated by the climbing-image nudged elastic band (CI-NEB) method (49). The vibration frequencies for all species were calculated to analyze thermodynamic contributions to free energies. The Gibbs free energy (ΔG) at different temperatures is calculated with $\Delta G = \Delta E$ + ΔZPE – TΔS, where ΔE refers to electric energy difference, and ΔZPE is zero-point energy difference. T and ΔS are temperature and entropy differences, respectively. The enthalpy and entropic contributions are calculated within the harmonic approximation for surface species and the ideal gas approximation for gas-phase species. The formation energies (ΔE) of all the species (* $C_xH_yO_z$) are calculated relative to gaseous energies of H_2 , H_2O and CH_4 as $\Delta E_{CxH_yO_z} = E_{CxH_yO_z} -$ E_{slab} – [x*(E_{CH4} – 2E_{H2}) + y*(E_{H2})/2 + z*(E_{H2O} – E_{H2})], where E_{CXHyOZ}, E_{slab}, E_{CH4}, E_{H2}, and E_{H2O} denote the electronic energies of the adsorbed intermediate over the surface, clean surface slab, methane, hydrogen molecule, and water, respectively.

Acknowledgments

This work was supported by the National Key Research and Development Program of China (2022YFA0911900) and the National Natural Science Foundation of China (22273076); T.W. thanks for the start-up packages from Westlake University and the Kunpeng research fund from Zhejiang Province. We thank the Research Center for Industries of the Future (RCIF) at Westlake University for supporting this work. F.A.P. acknowledge support from the U.S. DOE, Office of Science, Office of Basic Energy Sciences, Chemical Sciences, Geosciences, and Biosciences Division, Catalysis Science Program to the SUNCAT Center for Interface Science and Catalysis. We thank Westlake University HPC Center for computation support.

References

- 1. P. Sabatier, J. B. Senderens, C. R. Acad. Sci. Paris. 134, 514-516 (1902).
- V. Shadravan, et al., Effect of manganese on the selective catalytic hydrogenation of CO_x in the presence of light hydrocarbons over Ni/Al₂O₃: An experimental and computational study. ACS Catal. 10, 1535–1547 (2020).
- 3. E. C. Ra, *et al.*, Recycling carbon dioxide through catalytic hydrogenation: Recent key developments and perspectives. *ACS Catal.* **10**, 11318–11345 (2020).
- 4. Y. Li, et al., Promoting CO₂ methanation via ligand-stabilized metal oxide clusters as hydrogen-donating motifs. *Nat. Commun.* **11**, 1–8 (2020).

- G. Centi, E. A. Quadrelli, S. Perathoner, Catalysis for CO₂ conversion: A key technology for rapid introduction of renewable energy in the value chain of chemical industries. *Energy Environ. Sci.* 6, 1711–1731 (2013).
- 6. J. Zhong, *et al.*, State of the art and perspectives in heterogeneous catalysis of CO₂ hydrogenation to methanol. *Chem. Soc. Rev.* **49**, 1385–1413 (2020).
- 7. H. Shin, K. U. Hansen, F. Jiao, Techno-economic assessment of low-temperature carbon dioxide electrolysis. *Nat. Sustain.* **4**, 911–919 (2021).
- 8. M. C. O. Monteiro, M. F. Philips, K. J. P. Schouten, M. T. M. Koper, Efficiency and selectivity of CO₂ reduction to CO on gold gas diffusion electrodes in acidic media. *Nat. Commun.* **12**, 1–7 (2021).
- 9. S. Vijay, *et al.*, Unified mechanistic understanding of CO₂ reduction to CO on transition metal and single atom catalysts. *Nat. Catal.* **4**, 1024–1031 (2021).
- 10. G. Xu, C. Cai, T. Wang, Toward Sabatier optimal for ammonia synthesis with paramagnetic phase of ferromagnetic transition metal catalysts. *J. Am. Chem. Soc.* **144**, 23089–23095 (2022).
- 11. K. Posthumus, The application of the van 't Hoff-le Chatelier-Braun principle to chemical equilibria. *Recl. Trav. Chim. Pays-Bas.* **52**, 25–35 (1933).
- 12. S. Rönsch, *et al.*, Review on methanation From fundamentals to current projects. *Fuel* **166**, 276–296 (2016).
- 13. W. J. Lee, et al., Recent trend in thermal catalytic low temperature CO₂ methanation: A critical review. Catal. Today **368**, 2–19 (2021).
- 14. M. A. Vannice, The catalytic synthesis of hydrocarbons from H₂/CO mixtures over the group VIII metals. *J. Catal.* **37**, 449–461 (1975).
- 15. L. Gao, *et al.*, Enhanced nickel-catalyzed methanation confined under hexagonal boron nitride shells. *ACS Catal.* **6**, 6814–6822 (2016).
- 16. C. Heine, B. A. J. Lechner, H. Bluhm, M. Salmeron, Recycling of CO₂: Probing the chemical state of the Ni(111) surface during the methanation reaction with ambient-pressure X-ray photoelectron spectroscopy. *J. Am. Chem. Soc.* **138**, 13246–13252 (2016).
- 17. G. A. Mills, F. W. Steffgen, Catalytic methanation. Catal. Rev. 8, 159–210 (1974).
- 18. P. Munnik, M. E. Z. Velthoen, P. E. De Jongh, K. P. De Jong, C. J. Gommes, Nanoparticle growth in supported nickel catalysts during methanation reaction Larger is better. *Angew. Chem. Int. Ed.* **53**, 9493–9497 (2014).
- 19. S. Chen, et al., Raising the CO_x methanation activity of a Ru/γ-Al₂O₃ catalyst by activated modification of metal–support interactions. *Angew. Chem. Int. Ed.* **59**, 22763–22770 (2020).
- 20. L. Lin, *et al.*, Reversing sintering effect of Ni particles on γ-Mo₂N via strong metal support interaction. *Nat. Commun.* **12**, 1–11 (2021).
- 21. C. Vogt, *et al.*, Unravelling structure sensitivity in CO₂ hydrogenation over nickel. *Nat. Catal.* **1**, 127–134 (2018).
- 22. Y. S. Xiao, *et al.*, Balancing free and confined metallic Ni for an active and stable catalyst—A case study of CO methanation over Ni/Ni–Al₂O₃. *J. Energy Chem.* **50**, 73–84 (2020).
- 23. E. Köck, M. Kogler, T. Bielz, B. Klötzer, S. Penner, In situ FT-IR spectroscopic study of CO₂ and CO adsorption on Y₂O₃, ZrO₂, and yttria-stabilized ZrO₂. *J. Phys. Chem. C.* **117**, 17666–17673 (2013).
- 24. S. Kattel, P. Liu, J. G. Chen, Tuning selectivity of CO₂ hydrogenation reactions at the metal/oxide interface. *J. Am. Chem. Soc.* **139**, 9739–9754 (2017).
- 25. M. A. Lucchini, A. Testino, A. Kambolis, C. Proff, C. Ludwig, Sintering and coking resistant core-shell microporous silica-nickel nanoparticles for CO methanation: Towards advanced catalysts production. *Appl. Catal. B Environ.* **182**, 94–101 (2016).
- 26. Y. Li, et al., Selective light absorber-assisted single nickel atom catalysts for ambient sunlight-driven CO₂ methanation. *Nat. Commun.* **10**, 1–9 (2019).
- 27. W. Zhen, B. Li, G. Lu, J. Ma, Enhancing catalytic activity and stability for CO₂ methanation on Ni@MOF-5 via control of active species dispersion. *Chem. Commun.* **51**, 1728–1731 (2015).
- 28. C. H. Tan, S. Nomanbhay, A. H. Shamsuddin, Y. Park, Current developments in catalytic methanation of carbon dioxide A review. *Front. Energy Res.* **9**, 1–7 (2022).

- 29. L. Zhang, *et al.*, CO removal via selective methanation over the catalysts Ni/ZrO₂ prepared with reduction by the wet H₂-rich gas. *Int. J. Hydrogen Energy* **43**, 15985–15994 (2018).
- 30. B. Zhao, *et al.*, Bimetallic Ni-Co nanoparticles on SiO₂ as robust catalyst for CO methanation: Effect of homogeneity of Ni-Co alloy. *Appl. Catal. B Environ.* **278**, 119307 (2020).
- 31. M. P. Andersson, *et al.*, Toward computational screening in heterogeneous catalysis: Pareto-optimal methanation catalysts. *J. Catal.* **239**, 501–506 (2006).
- 32. A. C. Lausche, *et al.*, On the effect of coverage-dependent adsorbate-adsorbate interactions for CO methanation on transition metal surfaces. *J. Catal.* **307**, 275–282 (2013).
- 33. M. P. Andersson, *et al.*, Structure sensitivity of the methanation reaction: H₂-induced CO dissociation on nickel surfaces. *J. Catal.* **255**, 6–19 (2008).
- 34. J. X. Liu, H. Y. Su, W. X. Li, Structure sensitivity of CO methanation on Co(0001), (1012) and (1120) surfaces: Density functional theory calculations. *Catal. Today* **215**, 36–42 (2013).
- 35. C. Zhi, R. Zhang, B. Wang, Comparative studies about CO methanation over Ni(211) and Zrmodified Ni(211) surfaces: Qualitative insight into the effect of surface structure and composition. *Mol. Catal.* **438**, 1–14 (2017).
- 36. M. F. Francis, W. A. Curtin, Mechanical stress combined with alloying may allow continuous control over reactivity: Strain effects on CO dissociation and subsequent methanation catalysis over Ni(211), Ni₃Fe(211), and NiFe(112). *J. Phys. Chem. C* **121**, 6113–6119 (2017).
- M. Deimel, K. Reuter, M. Andersen, Active site representation in first-principles microkinetic models: Data-enhanced computational screening for improved methanation catalysts. ACS Catal. 10, 13729–13736 (2020).
- 38. T. Wang, F. Abild-pedersen, Achieving industrial ammonia synthesis rates at near-ambient conditions through modified scaling relations on a confined dual site. *Proc. Natl. Acad. Sci. U. S. A.* **118**, 1–5 (2021).
- 39. S. Van Ho, P. Harriott, The kinetics of methanation on nickel catalysts. *J. Catal.* **64**, 272–283 (1980).
- 40. J. K. Nørskov, F. Abild-Pedersen, F. Studt, T. Bligaard, Density functional theory in surface chemistry and catalysis. *Proc. Natl. Acad. Sci. U. S. A.* **108**, 937–943 (2011).
- 41. M. Che, Nobel Prize in chemistry 1912 to Sabatier: Organic chemistry or catalysis? *Catal. Today* **218–219**, 162–171 (2013).
- 42. J. Bao, J. He, Y. Zhang, Y. Yoneyama, N. Tsubaki, A core/shell catalyst produces a spatially confined effect and shape selectivity in a consecutive reaction. *Angew. Chem. Int. Ed.* **47**, 353–356 (2008).
- 43. L. Gao, *et al.*, A nickel nanocatalyst within a h-BN shell for enhanced hydrogen oxidation reactions. *Chem. Sci.* **8**, 5728–5734 (2017).
- 44. G. Kresse, J. Furthmüller, Efficiency of ab-initio total energy calculations for metals and semiconductors using a plane-wave basis set. *Comput. Mater. Sci.* **6**, 15–50 (1996).
- 45. S. R. Bahn, K. W. Jacobsen, An object-oriented scripting interface to a legacy electronic structure code. *Comput. Sci. Eng.* **4**, 56–66 (2002).
- 46. J. Wellendorff, *et al.*, Density functionals for surface science: Exchange-correlation model development with Bayesian error estimation. *Phys. Rev. B Condens. Matter Mater. Phys.* **85**, 32–34 (2012).
- 47. J. Wellendorff, *et al.*, A benchmark database for adsorption bond energies to transition metal surfaces and comparison to selected DFT functionals. *Surf. Sci.* **640**, 36–44 (2015).
- 48. D. Joubert, From ultrasoft pseudopotentials to the projector augmented-wave method. *Phys. Rev. B Condens. Matter Mater. Phys.* **59**, 1758–1775 (1999).
- 49. G. Henkelman, B. Uberuaga, H. Joʻnsson, A climbing image nudged elastic band method for finding saddle points and minimum energy paths graeme. *J. Chem. Phys.* **113**, 9901–9904 (2000).

Figures

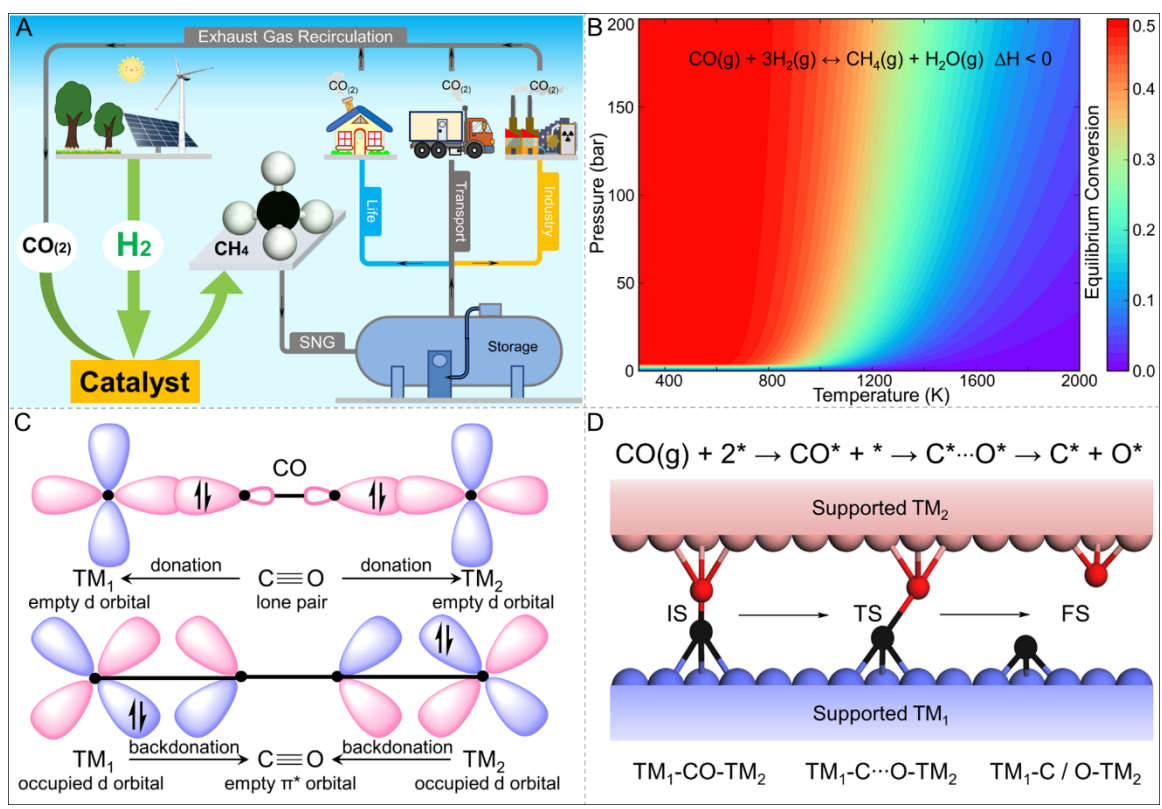


Figure 1. Key factors and challenges in CO methanation. (A) Carbon recycling through green hydrogen-based methanation, (B) Equilibrium conversion of stoichiometric CO and H₂ to methane and water at different temperatures and total pressures, (C) Molecular orbital model for the CO activation mechanism on dual sites, (D) Schematic structure of the ideal dual-site catalyst.

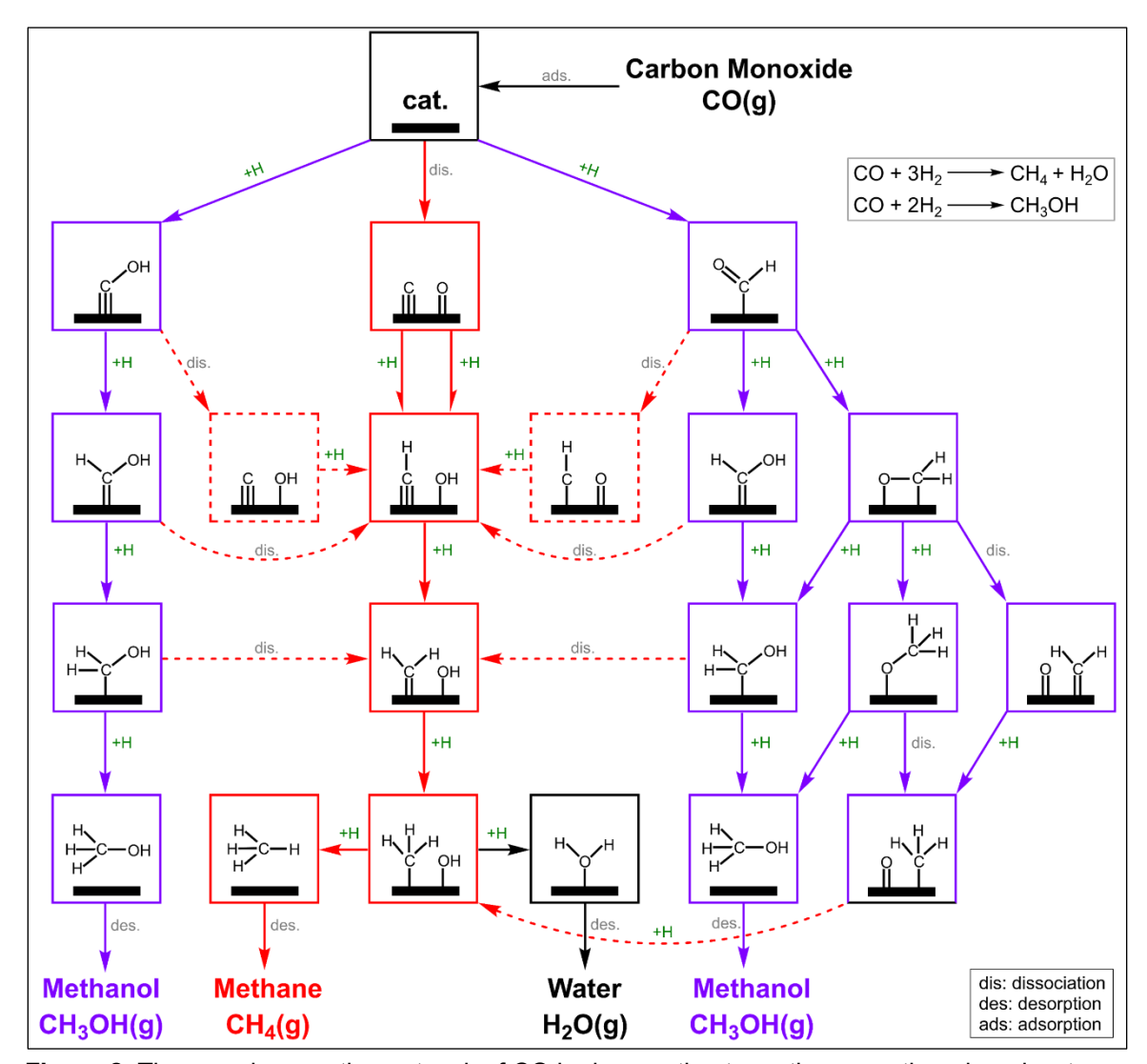


Figure 2. The complex reaction network of CO hydrogenation to methane, methanol, and water.

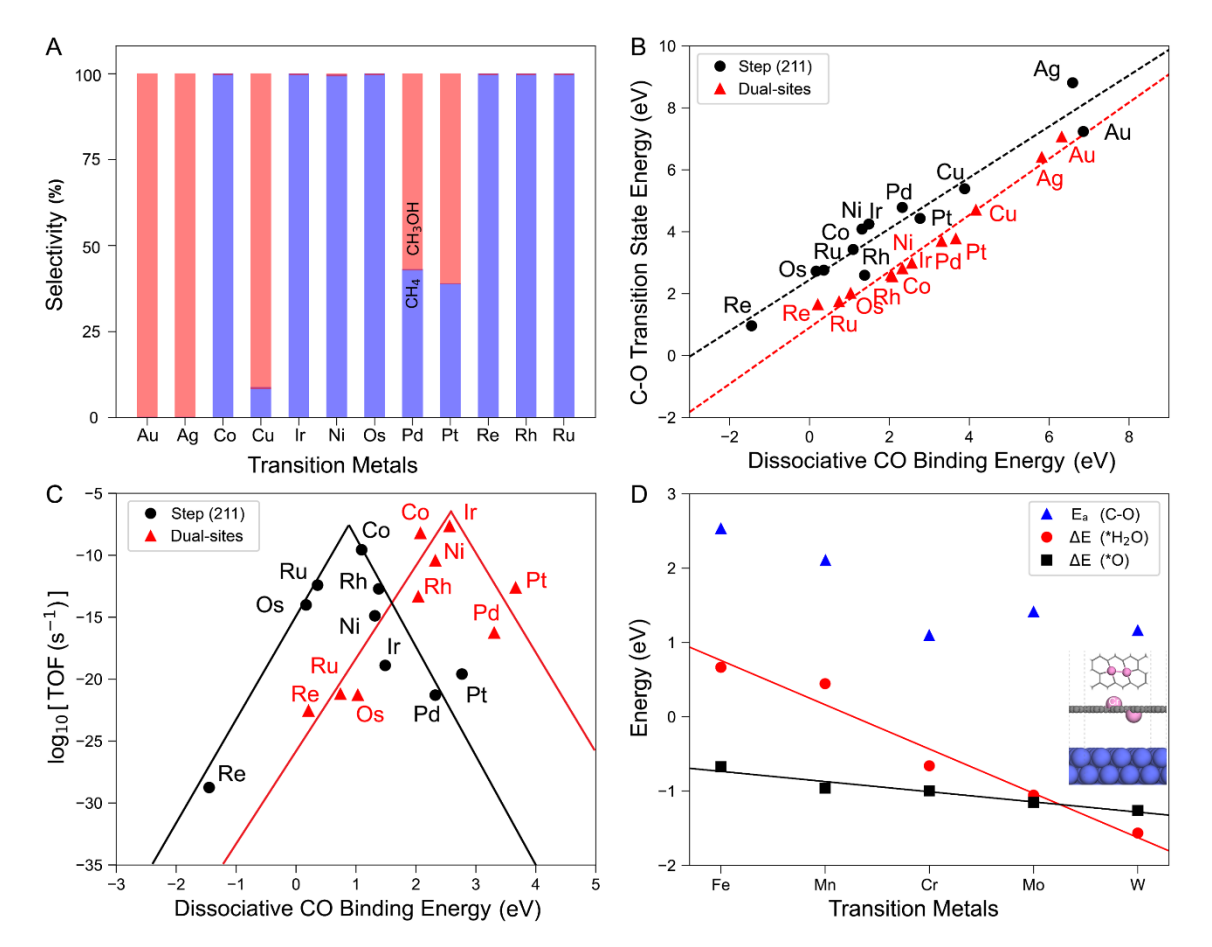


Figure 3. Comparative analysis of key properties. (A) Methane vs methanol selectivity on stepped (211) transition metal surfaces for CO hydrogenation at 523 K, p_{CO} = 1 bar, p_{H2} = 2 bar. (B) DFT calculated transition state energies of CO dissociation as a function of the dissociative adsorption energies of CO on the step sites (black circle) and dual sites (red triangles) on 12 transition metals. (C) Theoretically calculated TOF_{CH4} as a function of the dissociative adsorption energies of CO at 523 K, p_{CO} = 1 bar, p_{H2} = 2 bar. (D) The barrier for CO dissociation and the binding energies of *O/*H₂O on five Co-M₂/graphene dual-site catalysts.

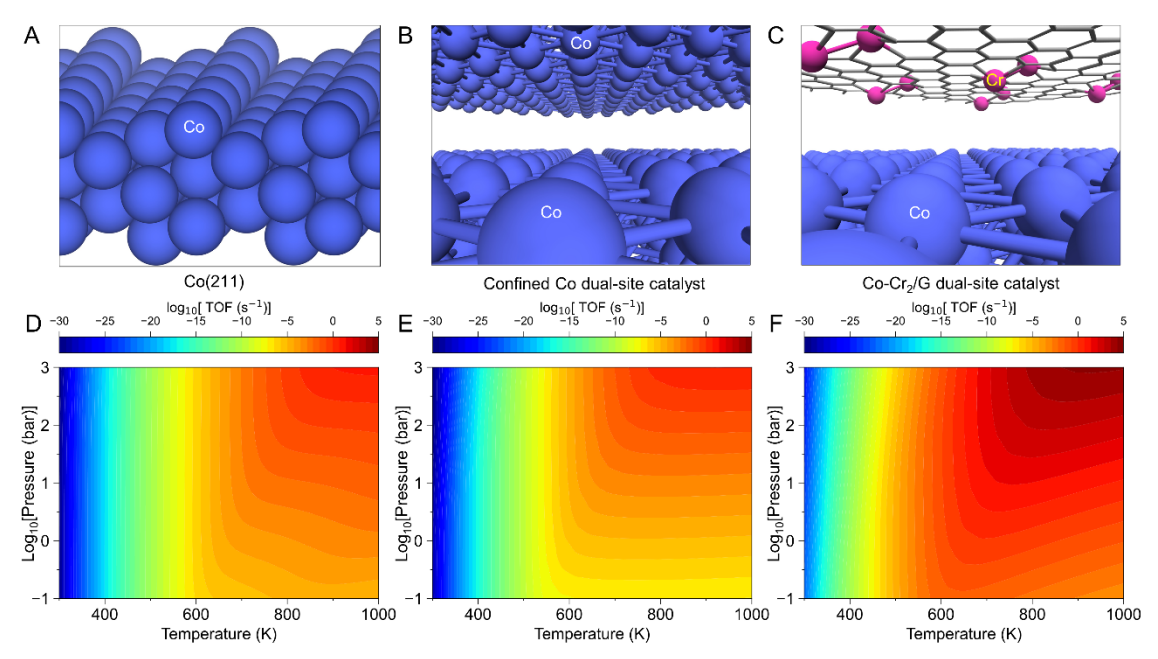


Figure 4. Schematic structures of (A) a stepped Co(211) surface, (B) a confined Co dual-site catalyst, and (C) a Co-Cr₂/G dual-site catalyst. Figures D, E, and F show the calculated TOF of CH₄ as a function of temperature and total pressure (p_{CO} : p_{H2} = 1/2), on the Co(211) surface, the Co dual-site catalyst, and the Co-Cr₂/G dual-site catalyst, respectively.